Journal of Power Sources 241 (2013) 259–265

Contents lists available at SciVerse ScienceDirect

Journal of Power Sources

journal homepage: www.elsevier.com/locate/jpowsour

Directly electrospinning growth of single crystal Cu_2ZnSnS_4 nanowires film for high performance thin film solar cell

Lin-Jer Chen [a,*], Yu-Ju Chuang [b]

[a] Institute of Electro-Optical Science and Engineering, National Cheng Kung University, Tainan 701, Taiwan
[b] Department of Materials Science and Engineering, National Cheng Kung University, Tainan 701, Taiwan

HIGHLIGHTS

- Cu_2ZnSnS_4 thin film is a candidate for low cost absorber layer in thin film solar cell.
- Electrospinning is one of the most promising methods for the fabrication of nanostructure materials.
- The continuous PVB/CZTS organized wires can be transformed to the CZTS nanowires via annealing.
- We report the first synthesis of I_2–II–IV–VI_4 nanowires and demonstrate their use in the fabrication of solar cells.

ARTICLE INFO

Article history:
Received 28 December 2012
Received in revised form
24 April 2013
Accepted 26 April 2013
Available online 4 May 2013

Keywords:
Electrospinning
Polyvinylbutyral
Kesterite
Semiconductor

ABSTRACT

Quaternary kesterite-type Cu_2ZnSnS_4 nanowires can be used as absorbing materials for thin film solar cells. The structural, morphological, compositional, and optical properties of the CZTS nanowires have been studied using X-ray diffraction (XRD), UV–vis spectroscopy, scanning electron microscopy (SEM), transmission electron microscopy (TEM) and optical absorption techniques respectively. The Cu_2ZnSnS_4 nanowires, fabricated by electrospinning process and sintered at 600 °C in Argon atmosphere, the cells exhibits a power conversion efficiency of 6.18% under AM 1.5 solar irradiation in the thin film solar cells. This study suggests that the optimized Cu_2ZnSnS_4 composite nanowire is a promising absorbing material for high performance solar cells.

1. Introduction

High-quality semiconductor nanoparticles consisting of abundant elements of low cost are of great interest for large-scale commercial applications. In order to promote the use of photovoltaic devices, it is necessary to develop low-cost solar cells with high efficiency, and less environmental impact. A quaternary Cu_2ZnSnS_4 (CZTS) thin film is a promising candidate for low cost absorber layer in thin film solar cell due to its excellent material properties for obtaining high efficiency. Recently, it has been reported by several research groups that CZTS nanoparticles were prepared via a precipitation reaction in hot organic solutions [1–3]. In addition, CZTS nanocrystals were prepared by solution-based synthesis [4,5] and were recently used for the fabrication of CZTS absorber films in photovoltaic devices [6]. However, these methods have some drawbacks such as expensive precursors, complicated apparatus and even some toxic byproducts evolved during their synthesis. Particularly, these methods are performed at high temperatures, which results in inter-diffusion of the component elements, and degrading the device quality structures [7,8].

This semiconductor combines the properties for an ideal absorber layer for photovoltaic applications, like a direct band gap of about 1.4–1.5 eV [5–7] and an optical absorption coefficient higher than 1×10^4 cm^{-1} [9,10]. The discovery of efficient multiple exciton generation by single photons in semiconductor nanoparticles has initiated intensive research to fabricate highly efficient solar cells in which the efficiency of solar light energy conversion theoretically reaches ca. 60% [11,12], which is much higher than that of conventional thin film solar cells.

The electrospinning technique is one of the most promising methods for the fabrication of 1D nanostructure materials [13]. Research on the synthesis of various inorganic and metal-oxide nanowires via electrospinning has recently increased [14,15]. The electrospinning route is a simple, versatile, and relatively inexpensive

* Corresponding author. Tel.: +886 922 640510; fax: +886 6 2096242.
E-mail address: linjerchen@hotmail.com (L.-J. Chen).

0378-7753/$ – see front matter © 2013 Elsevier B.V. All rights reserved.
http://dx.doi.org/10.1016/j.jpowsour.2013.04.128

technique for the synthesis of a broad range of hybrid nanocomposites. Unlike other methods produce short nanorods or nanotubes, with the electrospinning technique it is possible to produce continuous nanowires and nanotubes [8]. Although electrospinning has been used mainly for the fabrication of organic polymeric nanowires, ceramic metal-oxide nanowires has also received considerable interest due to their potential applications in areas including photovoltaic devices, piezoelectric materials, gas sensors, and solar cells [16–19]. Polyvinylbutyral (PVB) has been commonly used as capping agent. PVB is a nontoxic, odorless, and environmentally friendly polymer that is widely used as a functional material in various fields [20]. Due to its good compatibility with inorganic materials, PVB is an excellent organic component for the fabrication of organic/inorganic hybrid composites. To the best of our knowledge, CZTS nanowires synthesis using electrospinning routes has not been reported previously. Our synthesis marks an advance for kesterite quaternary semiconductor nanowires and offers a possible template by electrospinning process. Here, we report the first synthesis of I_2–II–IV–VI_4 nanowires and demonstrate their use in the fabrication of solar cells.

2. Material and methods

All chemicals were used as received without further purification. Copper (II) chloride ($CuCl_2$; 99.99%), elemental sulfur powder (98%) from Sigma Aldrich; zinc (II) chloride ($ZnCl_2$; 99.5%) from Alfa, tin (II) chloride ($SnCl_2$; 99.5%) from Mallinckrodt; ethanol absolute and hydrochloric acid (36.5%) were from PA Panreac; Polyvinylbutyral (PVB) (average M_v ~40 kDa) was obtained from ChangChun Group Company.

Typically, 2 mmol of $CuCl_2$, 4 mmol of elemental Sulfur, 1 mmol of $ZnCl_2$ and 1 mmol of $SnCl_2$, 20 wt.% PVB (PVB/ethanol content ratio = 2:8), 30 ml ethanol absolute and 1 ml hydrochloric acid (36.5%) to a 50-ml three-neck flask with attached condenser and stopcock valve in a nitrogen-filled glovebox, while magnetically stirred at room temperature for 2 h, followed by N_2 bubbling at 60 °C for 2 h while stirring to obtain a homogenous precursor of PVB/CZTS composites. In the electrospinning of polymer solutions, the wire formation process is characterized by the formation and thinning of the liquid jet and the solidification and deposition of wires on the collection target. A stainless steel electrode was connected to a high voltage power supply, which can generate a DC voltage of up to 30 kV. The applied voltage between the tip and collector were set at 18 kV with a tip-to-collector distance of 15 cm. The applied voltage overcomes the liquid surface tension to form a jet, which then bends and spirals into a large looping path as it thins into fine wires and solidifies. Homogenous precursor solutions of PVB/CZTS composites were prepared and used immediately for electrospinning. Because during this procedure evaporation of solvent occurred and this, in turn, results in a faster increase in the viscosity of the solution [21]. Also, the precursor solutions are immediately used for solvent evaporation as the production of the fibers becomes more rapid. Finally Cu_2ZnSnS_4 nanowires were obtained after annealing at 600 °C for 2 h.

The as-prepared samples were characterized by X-ray powder diffraction (XRD), scanning electron microscopy (SEM), thermogravimetric analysis (TGA), and transmission electron microscopy (TEM). XRD was carried out on a D/MAX-500 X-ray powder diffraction system with Cu Ka radiation (λ = 1.5418 Å). A scanning rate of 0.02° was applied to record the patterns in the 2 Theta range of 15–80°. TEM characterization was conducted on a JEM-2000EX system using an acceleration voltage of 160 kV. A Hitachi scanning electron microscopy (SEM) with at an acceleration voltage of 5 kV was employed to characterize the morphology.

3. Results and discussion

Fig. 1a–e shows a series of SEM images of PVB/CZTS nanowires obtained from precursor solutions with concentration ratios of 5 wt.%, 10 wt.%, 15 wt.%, 20 wt.%, and 25 wt.% (PVB/ethanol content ratio). As can be seen in Fig. 1(a), fewer wires were obtained when the ratio was 5 wt.%. When the concentration of PVB was 15 wt.%, bead-on-string structures were not produced. Usually, by increasing the concentration of the solution, the fiber size is also increased, due to increase in the viscosity [21]. It can be seen from Fig. 1 that fiber diameter increased with the increase of PVB ratio,

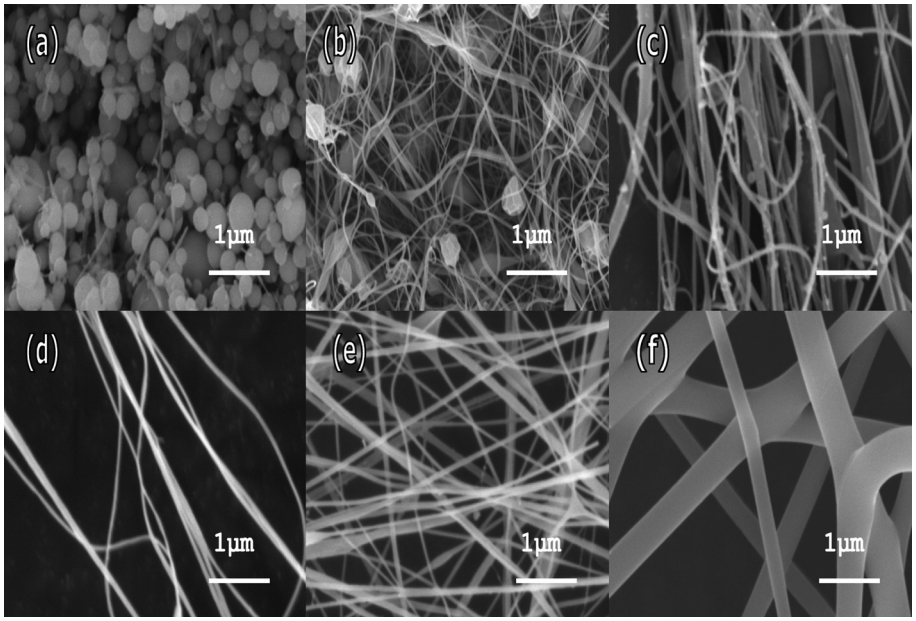

Fig. 1. SEM images of PVB/CZTS composite nanowires electrospinning from (a) 5 wt.%, (b) 10 wt.%, (c) 15 wt.%, (d) 20 wt.%, and (e) 25 wt.% aqueous solutions at 18 kV; (f) pure PVB fibers.

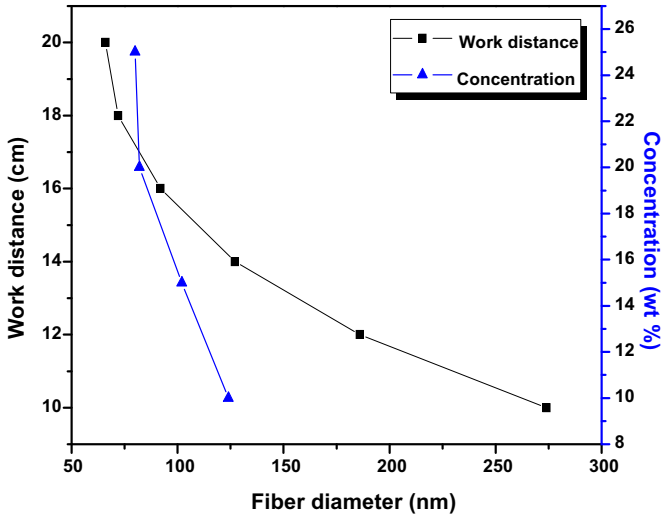

Fig. 2. Diameters of the PVB/CZTS composite wires for various work distances and concentration ratios. Other electrospinning operational parameters: 20 μL min^{-1} and 18 kV.

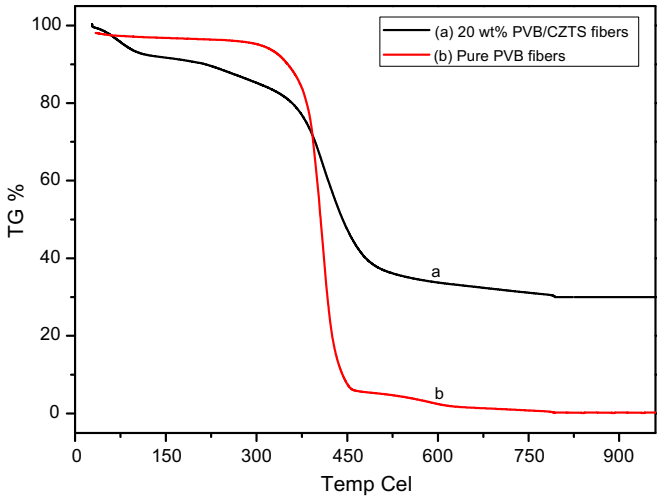

Fig. 4. Thermogravimetric analysis (TGA) curves of PVB/CZTS nanowires. (a) 20 wt % PVB/CZTS wire and (b) pure PVB fiber.

and also the content of fibers increased. The higher charge then increases the force exerted on the jet and the mechanism that forms the beads [22]. When the ratio further increased, the beads on wires decreased. The results showed that high concentration preferred generated wires ratios increased. The high conductivity solvent is helpful to the ion diffusion and reduces resistance. The high viscosity solvent can cause the diffusion of ions not to be easy, to reduce the conductivity [23].

When the concentration of PVB was increased, bead-on-string structures were observed, as shown in Fig. 1(b)–(e), and the bead density decreased. PVB/CZTS nanowires with smooth surfaces were obtained when the PVB/ethanol ratio was 20 wt.%. The concentration of PVB is thus a key factor in the preparation of PVB/CZTS composite nanowires. PVB acted as the capping agent, which in the PVB/CZTS composite nanowires exists states is adsorbed polymer chains induce not only static repulsion but also bridging attraction. The polymer usually carry specific functional groups to anchor them onto the surface of synthesized CZTS nanowires, thereby reducing surface energy and preventing grain growth. In addition to inhibiting grain growth and particle agglomeration, capping agents sometimes provide electrostatic and steric stabilization effects [24,25]. Polymer bridging is an agglomeration mechanism that is difficult to overcome. However, polymer bridging was less feasible due to the lack of specific interactions, such as H-bonding, between the solvent and the nanowires [26,27]. Pure PVB fibers are shown in Fig. 1(f); their morphology is smoother than those of PVB/CZTS wires.

Solution concentration and work distances were considered as the most important parameters affected the morphology remarkably in the electrospinning process. Obviously, as shown in Fig. 2, an increase in solution concentration and work distances caused a decrease on the average diameter of fibers. Uniform fibers with different diameters were obtained under different electrospinning concentrations in this experimental research scope. Cross-linking between fibers existed when obtained at lower spinning concentration, as shown in Fig. 1. The higher the concentration, the more sufficient the PVB/CZTS molecule chains entangle, which would make the electrospinning easier and diameter decrease. At a

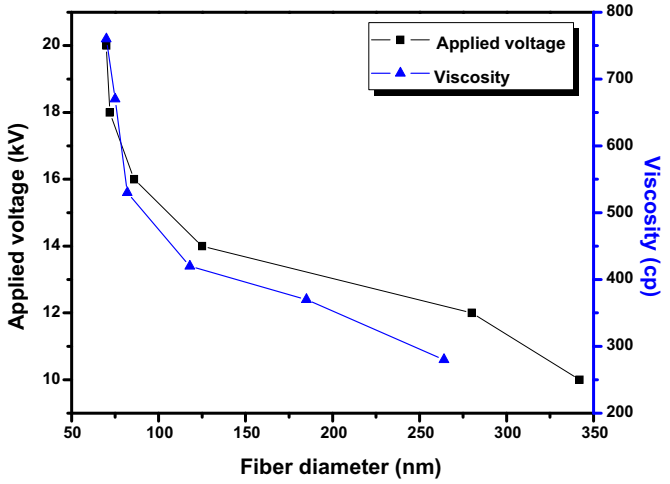

Fig. 3. Diameters of the PVB/CZTS composite wires for various viscosities and applied voltages. Other electrospinning operational parameters: 20 μL min^{-1}, 18 cm and 20 wt.% of PVB.

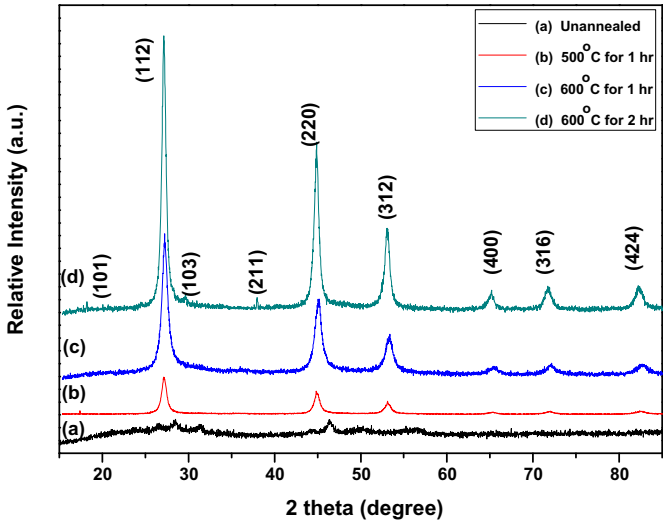

Fig. 5. XRD patterns of quaternary CZTS nanocrystals synthesized by the electrospinning process obtained from (a) 20 wt.% composite, after annealing at (b) 500 °C for 1 h, (c) 600 °C for 1 h, and (d) 600 °C for 2 h.

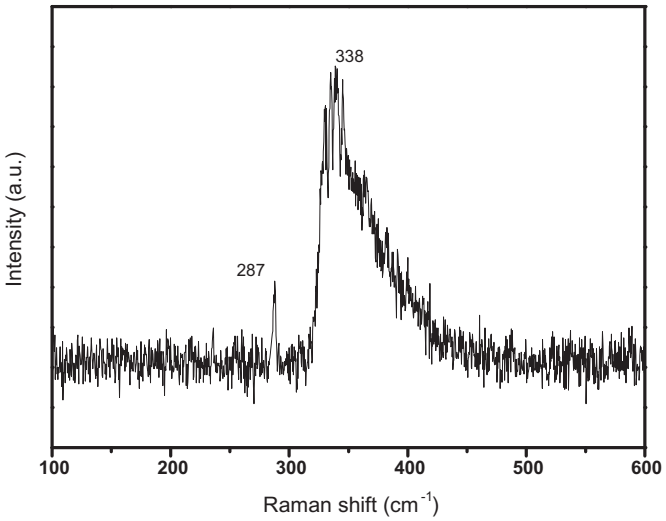

Fig. 6. Room temperature Raman spectrum of the as-prepared nanowires.

decreased distance, thicker wires were observed due to the reduced jet path will result in larger diameter because of less stretching of the solution [28]. Therefore, concentration and work distances were found to be the most important parameter influencing the fiber diameter in the electrospinning process.

Fig. 3 shows wire diameters of 20 wt.% PVB/CZTS composite wires for various viscosities and applied voltages (10 kV, 15 kV, 18 kV, and 20 kV). The wire diameter decreased with increasing viscosity, as expected (Fig. 3, black line). One hundred PVB/CZTS composite wires were selected from ten spots of 60 × 60 μm^2 to measure the distribution of the diameters. This may be due to the greater expanded conformation of PVB/CZTS in the solution caused by the electrostatic repulsion between PVB/CZTS mixture molecules. The molecular entanglement of PVB/CZTS in solution is thus expected to be higher. It was observed that the diameter distribution of the PVB/CZTS composite wires decreased with increasing applied voltage (Fig. 4, blue line, in web version). The jet is driven by a high electrical potential applied between the collector and the solution. The electrical forces which stretch the wires are resisted by the elongation viscosity of the jet. A reduction in size with the applied voltage has been reported for various electrospinning organic wires [29].

Fig. 4 shows TGA thermogram of the 20 wt.% PVB/CZTS nanowires. It was observed that the weight substantially decreases in the low temperature region. PVB/CZTS nanowires (Fig. 4(a)) exhibited three steps and a total loss of ca. 61.09%. The first step of ca. 10.27%, from 90 to 320 °C, can be attributed to the loss of volatile water and ethanol solution. The higher thermal stability of PVB/CZTS wires might be attributed to its higher chain compactness due to the interaction between the PVB and the CZTS materials [30]. The second significant weight loss of ca. 46.05%, between 320 and 500 °C, can be attributed to the loss of crystal water and the decomposition of acetate along with the degradation of PVB by dehydration on the polymer side chain [31]. The third step, which started at about 500 °C and ended at about 640 °C was a weight loss of ca.4.77%, which was assigned to the release of water formed from the condensation of carbonyl groups in the PVB/CZTS framework and the decomposition of the excess chalcogen species [32–34]. It is clear from the TG curve that all the PVB and the organic group were removed completely at 680 °C, resulting in a metal oxide composite phase [35–37]. The weight loss of PVB fibers (Fig. 4(b)) began to occur at approximately 350 °C and was complete at about 450 °C. The significant rapid rate of weight loss of ca. 76.65% in the temperature range of 338–449 °C, can be indicating to achieve the complete burn-out below 450 °C [38].

Table 1
Measured CZTS nanocrystal composition after annealing.

Sample	Precursor atomic ratio Cu:Zn:Sn:S	Measured by EDS[a] Cu:Zn:Sn:S (Zn/Sn)	Measured by ICPMS[b] Cu:Zn:Sn:S (Zn/Sn)
1	2:1:1:4	2:0.88:0.92:3.75 (0.956)	2:0.95:0.93:3.84 (1.021)
2	2:1.5:0.5:4	2:1.32:0.41:3.81 (3.219)	2:1.44:0.43:3.95 (3.348)
3	2:0.5:1.5:4	2:0.38:1.42:3.77 (0.267)	2:0.45:1.48:3.89 (0.304)

[a] EDS measurements have an error of ca. ±2 atom %.
[b] ICPMS measurement has an error of ±0.2 atom % for Zn, ±0.1 atom % for Sn, ±0.5 atom % for S. The sample 1 was used for the solar cell preparation.

Fig. 5 shows the XRD patterns of CZTS wires obtained from (a) 20 wt.% PVB/CZTS nanowires (b) after annealing at 500 °C for 1 h and (c, d) after annealing at 600 °C for 1 h, 2 h. Fig. 5 shows the XRD pattern of CZTS nanowires were used; five peaks corresponding to (112), (204)/(220), (116)/(312), (008)/(400), and (316)/(332) of the kesterite crystal structure, respectively, can be observed. All of the diffraction peaks can be indexed as the tetragonal kesterite phase of Cu_2ZnSnS_4 (JCPDS 26-0575), which implies that pure CZTS was synthesized. Thus, in order to determine that the nanocrystals are kesterite, it is crucial to be able to observe the minor peaks that are unique to the kesterite structure. For instance, the minor peaks at 18.20°, 29.67°, and 37.96° corresponding to the 101, 103, and 211

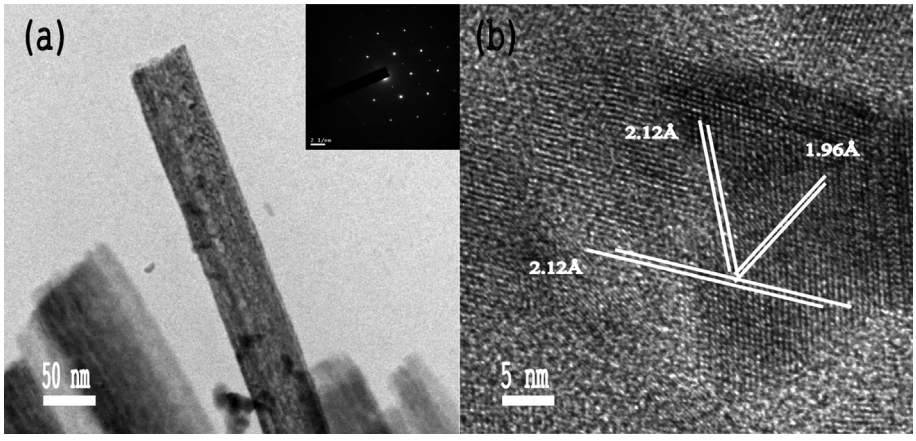

Fig. 7. TEM images of (a) as-synthesized CZTS nanostructures and SAED pattern (inset) and (b) high-resolution TEM of wire-like CZTS nanostructures recorded along [221].

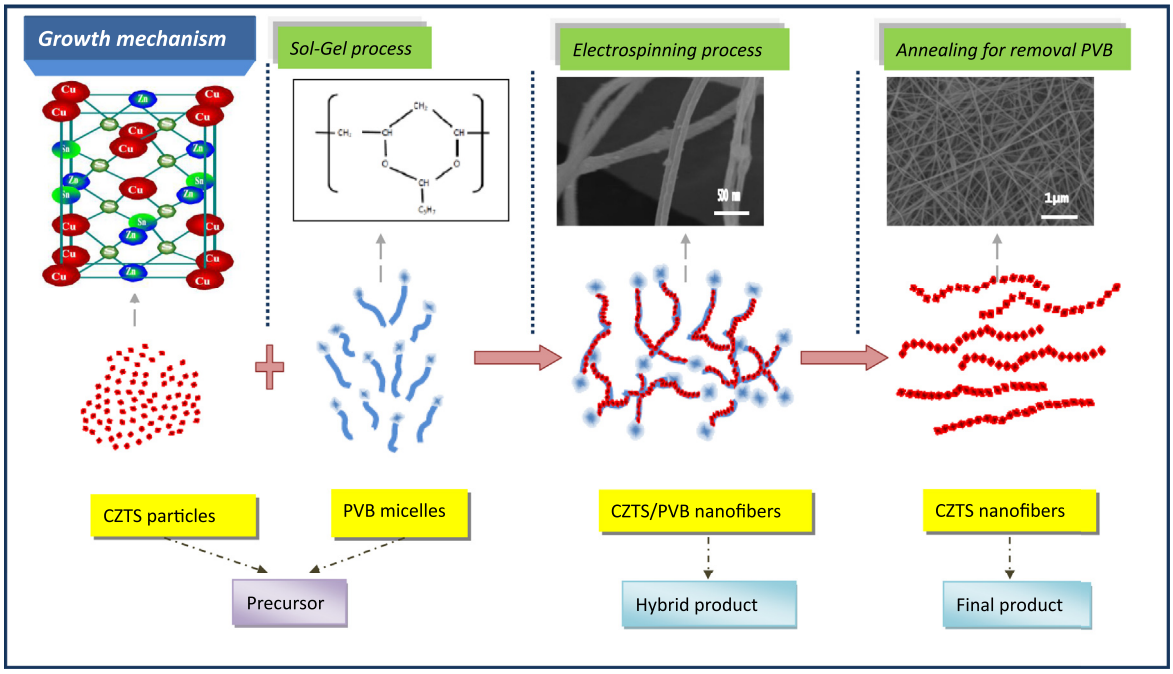

Fig. 8. Schematic illustration of the proposed growth mechanism for kesterite quaternary semiconductor CZTS nanowires.

peaks, respectively, are unique to the kesterite structure and are shown as a Fig. 5(d). However, after annealing at 600 °C for 1 h and 2 h, a single phase of well-crystallized CZTS with a tetragonal kesterite structure was obtained. A kesterite crystalline structure formed in the CZTS nanowires with the addition of PVB to the electrospinning step after annealing. As seen from the XRD pattern of as-prepared CZTS, the peak intensity of (112) was stronger than that of (220), revealing that the (112) was the preferred growth plane compared to the standard XRD pattern of CZTS [39]. Except for these peaks, no characteristic peaks were detected for other impurities, such as ZnS, CuS or Cu_2S. The CZTS nanowires sizes (D, nm) were calculated using the Scherrer equation ($D = K\lambda/\beta\cos\theta$) using the shape factor $K = 0.89$ and the $\lambda = 1.5406$ Å (CuKα1 source). Although XRD identified the phases, they can not be distinguished clearly because the 2θ positions of the kesterite CZTS or secondary phases, such as Cu_2SnS_3 and ZnS, are similar [40,41]. The nanowires were analyzed by the Raman spectra at room temperature to confirm the kesterite CZTS or secondary phases [42]. Fig. 6 shown a strong peak at 287 cm^{-1} and a weak peak at 338 cm^{-1} and agreeing well with those of bulk CZTS, which is consistent with the reported values of the characteristic peak of kesterite CZTS [43]. On the other hand, the characteristic Raman peak of zinc sulfide ZnS at 356 cm^{-1} is absent in the spectrum [44], suggesting that the XRD diffractions should not result from such a phase. Characteristics peaks from the other impurities such as binary and ternary sulfides are not observed. The lattice parameters calculated for the CZTS nanocrystals based on the (204) and (112) XRD peaks are 5.428 ± 0.002 and 10.842 ± 0.002 Å for a and c respectively, with the $c/2a$ ratio of 0.998 ± 0.002. The observed lattice parameters and $c/2a$ ratio agree very well with the reported values for the kesterite phase [1,6].

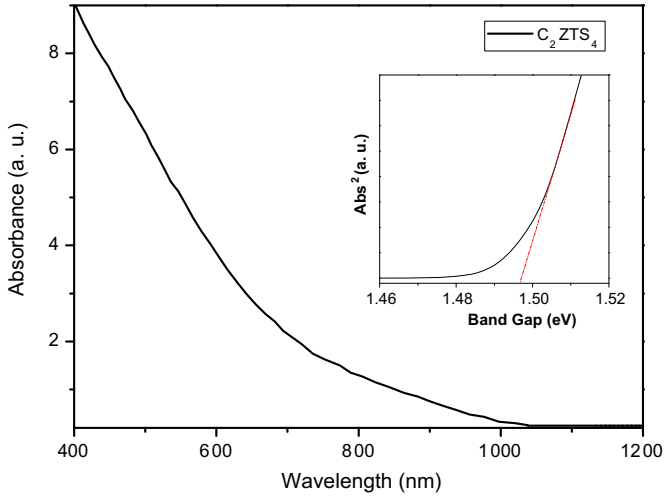

Fig. 9. UV–vis absorption spectrum of the as-synthesized CZTS nanocrystals in hexane. Inset shows the abs^2 vs eV for the CZTS nanocrystals; the estimated band gap energy is 1.48 eV.

The morphology of the CZTS nanowires was characterized using a transmission electron microscope (H-800) with an acceleration voltage of 160 kV. Fig. 7(a) shows TEM micrographs of CZTS nanowires by electrospinning at 18 kV. The wire-like morphology of CZTS can be seen. The wire-like nanostructures have diameters from 80 to 90 nm and lengths from hundreds of nanometers to several micrometers. By changing the reaction concentration, tip-to-collector distance, viscosity, and applied voltage, the nanowire size can be easily controlled. When the PVB/ethanol ratio was increased from 10 wt.% to 25 wt.% with a tip-to-collector distance of 15 cm, the diameters decreased to about 75 nm. The growth directions for the nanowires were determined from the selected area electron diffraction (SAED) patterns shown in the inset in Fig. 7(a). A high-resolution bright field TEM image of characteristic nanowires (80 nm) from the kesterite synthesis is shown in Fig. 7(b). The image is taken along the [221] zone axis with the $(2\bar{2}0)$, $(\bar{2}04)$, and $(0\bar{2}4)$ crystallographic planes indicated by white lines. Spacing measurements based on 6 planes indicated d-spacings of 1.92 ± 0.02 Å for the $(2\bar{2}0)$ and 1.91 ± 0.02 Å for the $(\bar{2}04)$ and $(0\bar{2}4)$. The measured angle between the $(2\bar{2}0)$ and $(0\bar{2}4)$ planes is

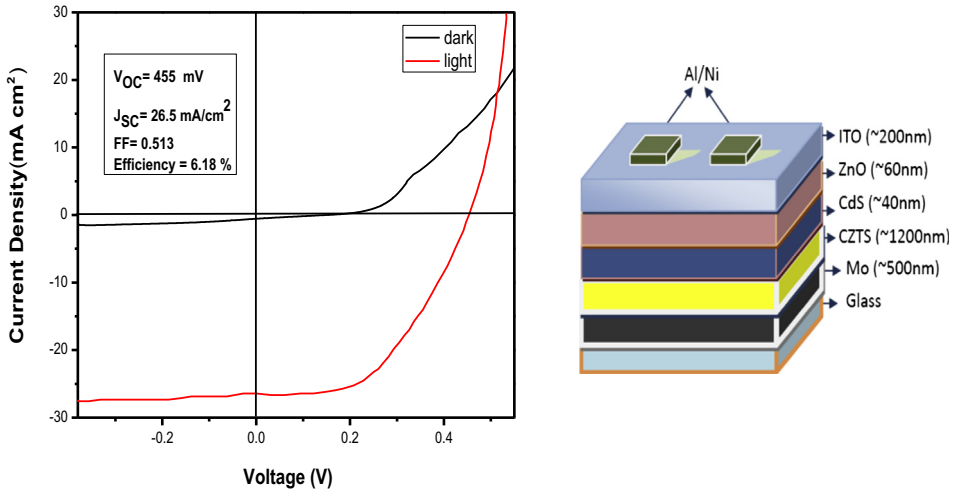

Fig. 10. Current–voltage characteristics by the AM 1.5 irradiation (100 mW cm^{-2}). The nanocrystal absorber layer was 1200 nm thick.

56.5 ± 0.5° and is 62 ± 0.5° between $(\bar{2}04)$ and $(0\bar{2}4)$ planes. If the structure were sphalerite, the measured angles should be 60° between all three planes, and the measured *d*-spacings should be 1.98 Å. These observed differences provide additional evidence of lattice distortion that result from cation ordering and the kesterite crystal structure. The zone axis of the SAED pattern was determined to be [221], and the pattern is typical for nanocrystals from this same synthesis procedure. These extra spots correspond to 2/3 the distance of the $(\bar{1}\bar{1}4)$ or $(1\bar{2}2)$ fundamental reflections and have a *d*-spacing of 3.3 Å. Both high-resolution TEM (Fig. 7) and XRD (Fig. 6) confirmed that the nanocrystals are crystalline with tetragonal kesterite structure. No other crystal phases were observed in the XRD patterns of the product. Compositional analysis by ICPMS showed that the average composition of the nanocrystals in the sample 1 has a molar Cu/Zn/Sn/S ratio of 2:1:1:4 and the composition of individual particles measured by EDS were 2:1:1:4 with a variation from particle to particle less than the experimental error of ca. ±2 atom % (see Table 1).

Based on the experimental observations above, a mechanism for the PVB template formation of the CZTS nanowires by electrospinning is proposed as shown in Scheme 1 of Fig. 8. PVB self-organizes into micelles (Fig. 8) because of its polar hydrophilic heads and hydrophobic alkyl chains. Inorganic species such as Cu^{2+}, Zn^{2+}, Sn^{4+}, and S^{4-} enter into and incorporate these PVB micelles. Clearly, the ordered polymer bundles can serve as seeds to result in further growth of the 1D CZTS nanowires for the template formation process. PVB is a highly adhesive agent and is commonly used as a polymer binder to form inorganic hybrid at room temperature for electrospinning processing [45–48]. The subsequent nucleation and crystal growth of CZTS occur in the micelles, leading to the formation of uniform and robust CZTS nanowires after the removal of PVB polymer. Using the proposed mechanism we can also explain the formation of the nanowire network. Electrospinning process is likely to play the major role in formation of the 1D nanostructure, therefore the conditions are favorable for CZTS nanowire network structure formation and for further developed PVB polymer at the end.

Fig. 9 shows UV/vis absorption spectra and optical micrographs of the kesterite quaternary CZTS nanocrystals synthesized by an electrospinning process and annealing at 600 °C for 2 h. The band gap energy determined from absorbance spectra (Fig. 9) of optically clear dispersions of nanocrystals was found to be 1.48 eV (837 nm), which is in good agreement with the reported literature [49]. The absorber layer may be formed simply by drop-casting on molybdenum coated soda-lime glass substrate. The films are annealed under flow of Ar at 500 °C for 3 h to remove the organic capping molecules. We fabricated the first batch of thin film solar cells in our laboratory using these films following chemical bath deposition of CdS layer, and RF sputtering of 60 nm intrinsic zinc oxide and 200 nm of ITO layers. The corresponding *I–V* characteristics of the solar cell are shown in Fig. 10. The final devices are scribed into small areas of 0.124 cm^2 with a small dap of silver paint applied to form the top contact. The device parameters for a single junction Cu_2ZnSnS_4 solar cell under AM1.5G are as follows: open circuit voltage of 455 mV, short-circuit current of 26.5 mA cm^{-2}, fill factor of 51.3%, and a power conversion efficiency of 6.18%.

4. Conclusions

Cu_2ZnSnS_4 nanowires were successfully fabricated via electrospinning. The continuous PVB/CZTS organized wires can be transformed to the CZTS nanowires via annealing. The wires are comprised of compact CZTS nanocrystals, maintaining their 1D identity. Tetragonal kesterite nanowires with a diameter of 80 nm can be produced and which is a single crystal with a growth direction of [221]. Active area cell efficiencies up to 6.18% (V_{oc} = 455 mV, J_{sc} = 26.5 mA cm^{-2}, FF = 0.513) have been demonstrated using the I_2–II–IV–VI_4 based absorber layer fabricated. These compositional, structural, and mechanistic findings provide valuable insight in the development of thin film solar cells using quaternary I_2–II–IV–VI_4 semiconductors.

Acknowledgments

This present study has been supported in part by National Science Council of Taiwan and the collaboration of Center for Micro/Nano Science and Technology of National Cheng Kung University.

References

[1] C. Steinhagen, M.G. Panthani, V. Akhavan, B. Goodfellow, B. Koo, B.A. Korgel, J. Am. Chem. Soc. 131 (2009) 12554–12555.
[2] Q.J. Guo, H.W. Hillhouse, R. Agrawal, J. Am. Chem. Soc. 131 (2009) 11672–11673.
[3] S.C. Riha, B.A. Parkinson, A.L. Prieto, J. Am. Chem. Soc. 131 (2009) 12054–12055.
[4] G.M. Ford, Q. Guo, R. Agrawal, H.W. Hillhouse, Chem. Mater. 23 (2011) 2626–2629.
[5] L.J. Chen, Y.J. Chuang, Mater. Lett. 91 (2013) 372–375.
[6] T.K. Todorov, K.B. Reuter, D.B. Mitzi, Adv. Mater. 22 (2010) E156–E159.
[7] L.J. Chen, J.D. Liao, Y.J. Chuang, CrystEngCommun 13 (2011) 2909–2914.

[8] M. Jeon, T. Shimizu, S. Shingubara, Mater. Lett. 65 (2011) 2364–2367.
[9] K. Ito, T. Nakazawa, Jpn J. Appl. Phys. 27 (1998) 2094–2097.
[10] Y.B. Kishore Kumar, G. Suresh Babu, P. Uday Bhaskar, V. Sundara Raja, Sol. Energy Mater. Sol. Cells 93 (2009) 1230–1237.
[11] R.D. Schaller, V.I. Klimov, Phys. Rev. Lett. 92 (2004) 186601.
[12] X. Zhou, S. Chen, D. Zhang, X. Guo, W. Ding, Y. Chen, Langmuir 22 (2006) 1383–1387.
[13] S. Cavaliere, S. Subianto, I. Savych, D.J. Jones, J. Rozière, Energy Environ. Sci. 4 (2011) 4761–4785.
[14] C. Shao, H. Guan, Y. Liu, R. Mu, J. Mater. Sci. 41 (2006) 3821–3824.
[15] O. Toprakci, L. Ji, Z. Lin, Hatice A.K. Toprakci, X. Zhang, J. Power Sources 196 (2011) 7692–7699.
[16] E. Zhmayev, D. Cho, Y.L. Joo, Polymer 51 (2010) 274–290.
[17] M. Wang, S.A. Vail, A.E. Keirstead, M. Marquez, D. Gust, A.A. Garcia, Polymer 50 (2009) 3974–3980.
[18] B. Ding, E. Kimura, T. Sato, S. Fujita, S. Shiratori, Polymer 45 (2004) 1895–1902.
[19] L.J. Chen, J.D. Liao, Y.J. Chuang, Y.S. Fu, J. Am. Chem. Soc. 133 (2011) 3704–3707.
[20] R.L. Feller, M. Curran, V. Colaluca, J. Bogaard, C. Bailie, Polym. Degrad. Stabil. 92 (2007) 920–931.
[21] J.M. Deitzel, J. Kleinmeyer, D. Harris, N.C. Beck Tan, Polymer 42 (2001) 261–272.
[22] H. Fong, I. Chun, D.H. Reneker, Polymer 40 (1999) 4585–4592.
[23] P. Ruenraroengsak, A.T. Florence, Int. J. Pharm. 298 (2005) 361.
[24] L. Guo, J. Nie, B. Du, Z. Peng, B. Tesche, K. Kleinermanns, J. Colloid Interface Sci. 319 (2008) 175–181.
[25] X. Sun, Y. Luo, Mater. Lett. 59 (2005) 3847–3850.
[26] Y. Otsubo, M. Horigome, Korea-Aust. Rheol. J. 15 (2003) 27–33.
[27] J. Swenson, M.V. Smalley, H.L.M. Hatharasinghe, Phys. Rev. Lett. 81 (1998) 5840–5843.
[28] D.H. Reneker, I. Chun, Nanotechnology 7 (1996) 216.
[29] S.G. Lee, S.S. Choi, C.W. Joo, J. Korean Fiber Soc. 39 (2002) 1.
[30] M.R. Karim, H.W. Lee, R. Kim, B.C. Ji, J.W. Cho, T.W. Son, W. Oh, J.H. Yeum, Carbohydr. Polym. 78 (2009) 336–342.
[31] Y.Y. Chen, W.C.J. Wei, J. Eur. Ceram. Soc. 21 (2001) 2535–2540.
[32] H. Zhang, H. Song, B. Dong, L. Han, G. Pan, X. Bai, L. Fan, S. Lu, H. Zhao, F.J. Wang, Phys. Chem. C 112 (2008) 25.
[33] W. Liu, D.B. Mitzi, M. Yuan, A.J. Kellock, S. Jay Chey, O. Gunawan, Chem. Mater. 22 (2010) 3.
[34] A.F. Lotus, R.K. Feaver, L.A. Britton, E.T. Bender, D.A. Perhay, N. Stojilovic, R.D. Ramsier, G.G. Chase, Mater. Sci. Eng. B 167 (2010) 55–59.
[35] J. Stejskal, P. Kratochvil, Langmuir 12 (1996) 3389.
[36] A. Riede, M. Helmstedt, V. Riede, J. Stejskal, Langmuir 14 (1998) 6767.
[37] M. Beaman, S.P. Armes, Colloid Polym. Sci. 271 (1993) 70.
[38] L.A. Salam, R.D. Matthews, H. Robertson, J. Eur. Ceram. Soc. 20 (2000) 1375–1383.
[39] A. Singh, H. Geaney, F. Laffir, K.M. Ryan, J. Am. Chem. Soc. 134 (2012) 2910–2913.
[40] C. Zou, L.J. Zhang, D.S. Lin, Y. Yang, Q. Li, X.J. Xu, CrystEngCommun 13 (2011) 3310–3313.
[41] M.L. Liu, F.Q. Huang, L.D. Chen, I.W. Chen, Appl. Phys. Lett. 94 (2009) 202103.
[42] M. Grossberg, J. Krustok, J. Raudoja, K. Timmo, M. Altosaar, T. Raadik, Thin Solid Films 519 (2011) 7403–7406.
[43] F. Liu, Y. Li, K. Zhang, B. Wang, C. Yan, Y. Lai, Z. Zhang, J. Li, Y. Liu, Sol. Energy Mater. Sol. Cells 94 (2010) 2431–2434.
[44] L. Shi, C. Pei, Y. Xu, Q. Li, J. Am. Chem. Soc. 133 (2011) 10328–10331.
[45] L.J. Chen, J.D. Liao, Y.J. Chuang, Y.S. Fu, Polymer 52 (2010) 116–121.
[46] D. Li, Y.N. Xia, Adv. Mater. 16 (2004) 1151.
[47] M. Law, J. Goldberger, P. Yang, Annu. Rev. Mater. Res. 34 (2004) 83.
[48] M. Wang, J.H. Yu, D.L. Kaplan, G.C. Rutledge, Macromolecules 39 (2006) 1102–1107.
[49] S.H. Wei, A. Zunger, J. Appl. Phys. 78 (1995) 3846–3856.